Boundary Analysis of Damping Methods for Virtual Synchronous Generators

Xi Luo, Yadala Pavankumar, Efstratios I. Batzelis, Abhinav Kumar Singh School of Electronics and Computer Science University of Southampton Southampton, U.K. xi.luo@soton.ac.uk Georgia Saridaki, Panos Kotsampopoulos, Nikos Hatziargyriou School of Electrical and Computer Engineering National Technical University of Athens Athens, Greece

Abstract— Virtual synchronous generators (VSGs) imitate traditional synchronous generators to provide virtual inertia and damping for inverter-based resources. The emulated damping relates to the power synchronization, therefore, has a major impact on system stability. Although various damping methods exist, phase-locked loop (PLL) integration is particularly concerning, as it is a key component in gridfollowing (GFL) control but now is being applied to gridforming (GFM). This paper analyzes the typical VSG control and PLL damping unit by mapping stability boundaries and feasibility range. The boundaries are mapped in two dimensions to determine the relationship between the control parameters and the grid impedance. A comprehensive sensitivity analysis of controller parameters for VSG stability is conducted, drawing parallels with the equivalence of droop-based GFM stability. Finally, the boundary analysis is verified by time-domain simulation results and demonstrates the reliability of dampingswitching method.

Keywords—Grid-forming inverter, virtual synchronous generator, damping emulation, phase-locked loop, grid strength.

I. INTRODUCTION

The growth of renewable energy technologies has made power systems more reliant on power-electronic interfaced generation, introducing low-inertia and poor-damping that impact the frequency stability and oscillatory stability of power systems with inverter-based resources (IBRs). As power systems continue to evolve, addressing these challenges has become essential. Inverters are typically operated in two control modes: grid-following (GFL) and grid-forming (GFM). Traditionally, the GFL operates as a current source, synchronizing to the grid frequency via a phase-locked loop (PLL) and regulating the output current to transfer a specified amount of active or reactive power [1]. In weak or low-inertia grids, such synchronization units may struggle to remain stable due to a lack of grid frequency support. A better alternative in weak grids is to use GFM mode, i.e. to act as a voltage source and actively form its own frequency and voltage output [2].

Existing control methods for GFM inverters emphasize *droop* and *virtual synchronous generator* (VSG) control. Most research adopts droop control [3] that linearly relates active and reactive power to frequency and voltage (P- ω and Q-V) for synchronization and load sharing. GFM with droop control normally has no inertia support, however, VSG can mimic the behavior of a real synchronous generator by applying the swing equation and thus providing inertia support to the whole system during transient process [4]-[6]. It incorporates the dynamic behavior of synchronous generators (SGs) into the power synchronization loop to regulate the energy stored in the power converter and associated energy storage DC links [7]. Thus, the power synchronization stability of VSG is strongly influenced by the design parameters, such as inertia *J*

and damping *D*, as well as control strategies like adaptive inertia support [8] and damping emulation [4], [9]. Although droop control and VSG are different control strategies, equivalence is established between the two methods [10], allowing droop control to be viewed as a special case of VSG control under certain assumptions.

Current research has explored the stability of GFL and GFM inverters with different grid strengths and suggests that GFL tends to be unstable in weak grids, while GFM may lose stability in strong grids [11]. VSG, as a type of GFM control, is also prone to become unstable in stiff grids [5], [6]. PLL is commonly used in GFL to track grid frequency, but it is also mentioned in some VSG variants to help with the damping effects [4] or current limitations [12] and improve dynamic performance. It was suggested in [13] that adding a transient damping term based on the PLL can prevent steady-state deviations in active output power during sudden grid frequency drops. However, authors in [4] noted that VSG damping methods that introduce PLL may affect the stability of weak grids, and [9] verified the negative impact of PLL in VSG. The limitations of PLL damping loop in GFM control are mentioned, but a comprehensive analysis under different grid strengths and quantified evaluation are still missing.

In order to better understand the dynamic behavior of the inverter, stability boundary methods have been proposed to visualize the upper and lower limits of system stability [14]. For example, [7] determined the feasible ranges of virtual inertia (*J*) and damping (*D*) from the stability boundaries of the VSG. [6] observed the boundary curves of *J* versus *D* and proposed online tuning inertia method. The effect of grid impedance on the tuning of VSG parameters is not clear - it can be further analyzed using stability boundaries.

This paper analyzes the performance of VSGs under different grid strengths by constructing stability boundaries that illustrate how PLL integration affects either positively or negatively the damping behavior depending on the grid strength. This approach quantifies the impact of PLLs on VSG stability. The main contributions are:

- Defining VSG stability boundaries to provide guidance for parameter selection;
- A comprehensive sensitivity analysis of VSG control parameters with respect to grid strength, assessing PLL's impact on damping; drawing comparisons with typical GFM droop control from the view of stability boundaries;
- Demonstrating the application of defined stability region by testing a damping-switching method via PLL activation/deactivation.

II. MODELLING

This study investigates a single-inverter single-infinite bus system, illustrated in Fig. 1. The inverter, operating in GFM

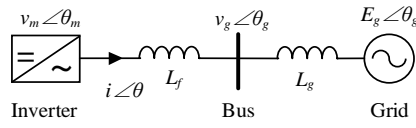


Fig. 1. Single-inverter-infinite-bus system.

mode, is connected to the grid through an inductance filter (L_f) . The primary focus is the application of the VSG control strategy, along with an exploration of different methods for enhancing damping performance. To facilitate a comparative analysis, the typical droop-based GFM control approach is also presented.

A. VSG and damping methods

Fig. 2(a) shows the outer power control loop that provides the voltage phase angle and magnitude to serve as the references for the VSG system. This is followed by inner loops that drive the inverter output via standard proportional-integral (PI) voltage and current controllers [1], [11]. The concept of VSG control is to emulate features of traditional synchronous generators (SG) using an inverter unit. The simplest model for synchronization relies on the conventional swing equation, as given by:

$$J\omega \frac{d\omega}{dt} = P_{ref} - P + P_{damp},\tag{1}$$

where P_{ref} and P are the inverter active power setpoint and measured values, J is the virtual inertia, and ω is the angular frequency of the VSG. It is worth mentioning that the damping power (P_{damp}) is often modelled as an approximation based on the frequency difference,

$$P_{damp} = D(\omega_g - \omega), \tag{2}$$

where D denotes the virtual damping coefficient, while the grid frequency ω_g (highlighted in Fig. 2(a)) can be set to either the nominal frequency ω_n [6], commonly used in VSG, or the measured frequency ω_m [9]. The measured frequency is often obtained from PLL [1] that tracks the system frequency by aligning the q axis voltage. The reactive power loop involves a Q-V droop module for voltage magnitude response, which incorporates a first-order low-pass filter (LPF) with cut-off frequency ω_c (= $2\pi f_c$) to filter the noises in measured power and a per unit droop gain m_q , defined by:

$$V - V_n = -m_q(Q - Q_{ref}), \tag{3}$$

Here, V_n and Q_{ref} refer to the system nominal voltage and reactive power reference set-point, respectively.

B. Droop-based control

The standard GFM controller with droop-based frequency response is shown in Fig. 2(b) [3]. In this configuration, the droop function serves both synchronization and power sharing response roles, actively forming the reference frequency and voltage. Similar to (3), the P- ω droop can be expressed as:

$$\omega - \omega_n = -m_p(P - P_{ref}). \tag{4}$$

Comparing the power synchronization loop of VSG with droop control reveals interesting insights. As outlined in [10], the droop method can be viewed as a special case of VSG by defining the droop gain m_p and LPF cut-off frequency ω_c based on the following relationships:

$$J = \frac{1}{\omega_c * m_p}; D = \frac{1}{m_p}. \tag{5}$$

III. STABILITY BOUNDARY ANALYSIS

Stability Boundary Tracking (SBT) algorithm is a viable

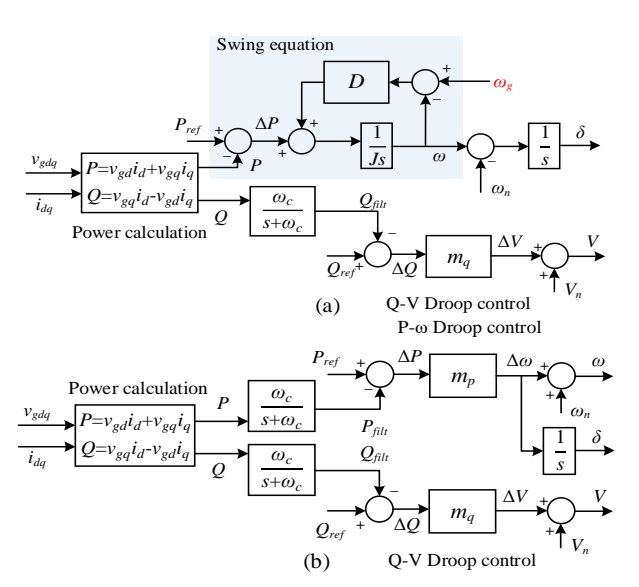


Fig. 2. Inverter GFM control scheme. (a) VSG and (b) droop-based control. Table I. Parameters of the system.

Parameters	Symbol	Values
System frequency	f_n	50 Hz
Base power	S_B	10 MVA
Inverter reference active power	P_{ref}	1 pu
Inverter reference reactive power	Q_{ref}	0.2 pu
System nominal voltage	V_n	1.01 pu
Virtual inertia	J	1.6 pu
Virtual damping factor	D	50 pu
Droop coefficient	m_q	5%
Low-pass filter cut-off frequency	f_c	5 Hz
PLL proportional gain	k_p	80
PLL integral gain	k_i	4000
Voltage control (VC) proportional gain	k_{pv}	5
Voltage control integral gain	k_{iv}	250
Current control (CC) proportional gain	k_{pi}	1.25
Current control integral gain	k_{ii}	10

approach to investigate system dynamic behavior by relating certain parameters of interest that render the system marginally stable. [14] introduces the SBT algorithm in detail, which is essentially a "grid search" method – sampling all relevant parameters and assessing stability status to form the multi-dimensional stability boundaries. The stability analysis, performed via MATLAB/Simulink, involves linearizing the model at multiple operating points, identifying eigenvalues, and using them to evaluate stability. Such analysis has been applied in this study to support the theoretical understanding and system parameter selection of VSG system.

This paper focuses on mapping the two-dimensional stability boundaries to identify the relationship between control parameters and grid impedance. The system stability is inferred from small-signal analysis that is repeated at different short circuit ratios (SCR) [15]. When the system changes from stable to unstable, or vice versa, the corresponding SCR value is captured as a boundary point. Notably, if the system fails to initialize the power flow, it will trigger a warning and be marked on the plots as well. Then, the controller parameter varies, and the boundary points can be collated together to form the stability boundary curve. To evaluate damping methods in VSG systems, this section compares two models: typical VSG model (VSG), which relies on nominal frequency for damping; and an alternative model using measured frequency via PLL (VSG+PLL). parameters of system components are listed in Table I.

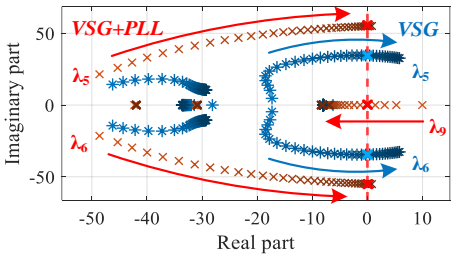


Fig. 3. Trace of low-frequency eigenvalues for increasing SCR.

Table II. Participation factor (PF) analysis at SCR=6.

	Mode	Damp. ratio	Freq. (Hz)	Major Participating States (with PF values)
VSG	5	0.084	5.69	δ_{GFM} (1); ω_{GFM} (0.78); VC_q (0.66)
VSG	6	0.084	5.69	δ_{GFM} (1); ω_{GFM} (0.78); VC_q (0.66)
VSG	5	0.18	8.58	δ_{GFM} (1); ω_{GFM} (0.94); ω_{PLL} (0.61)
+	6	0.18	8.58	δ_{GFM} (1); ω_{GFM} (0.94); ω_{PLL} (0.61)
PLL	9	1	0	VC_q (1); ω_{PLL} (0.93); δ_{GFM} (0.50)

A. Eigenvalue analysis

The trajectories of dominant eigenvalues with varying SCR from 2 to 10 are first explored; the remaining higherfrequency eigenvalues do not affect the stability and are omitted for simplicity. Fig. 3 depicts that reducing the grid impedance (i.e. increasing SCR) leads to the VSG system stability change. In the conventional VSG case (blue markers), a pair of eigenvalues (λ_5 , λ_6) shifts monotonically to the right half-plane, which yields the boundary point at an SCR of 6.93. Table II lists the critical eigenvalues with their damping ratios, frequencies and major participation factors (PF), where the frequencies are in the sub-synchronous range and depend mainly on the control synchronization loops. It can be found that the dominant eigenvalues are highly sensitive to the state variables, such as δ_{GFM} and ω_{GFM} , associated with the inverter system synchronization. The VSG, as a voltage source under current control, is therefore prone to current deviations and vulnerable to strong grids; this reaffirms literature that GFM may lose synchronization in stiff grids [1], [11].

However, the system with PLL (red markers) initially exhibits instability in a weaker grid strength due to the real eigenvalue λ_{9} lying on the right side. As the SCR increases, this eigenvalue moves towards the stable region and the boundary point is SCR=2.53. The PF analysis in Table II shows that λ_9 is sensitive to the additional state variable, ω_{PLL} , introduced by the PLL. The weakness of PLL has been widely reported, i.e., struggling with weak grids due to sensitivity to voltage disturbances [9], [11]. There is also a pair of eigenvalues (λ_5 , λ_6) as in conventional VSG, with higher damping ratios that shifted to the right. In the example case of SCR=6 shown in Table II, the damping ratios are increased from 8.4% to 18% compared to the conventional VSG. It can also be observed from the main participating states that the higher damping eigenvalues are aided by the PLL loop. The well damped system can therefore remain stable until the SCR exceeds 9.53. This observation has already been reported in [4], but without methodical characterization of the stability boundaries as follows.

B. Sesitivity analysis: J and D

Fig. 4 illustrates the mapped 2-D stability boundary curve for VSG systems, combining SCR with another key controller parameter, virtual inertia *J*. In the low-SCR range, the light red area represents where load flow fails to converge, creating an infeasible region. This region sets the first boundary line (yellow dashed line) – i.e., power transfer capability boundary line – which indicates the system has limited capacity to

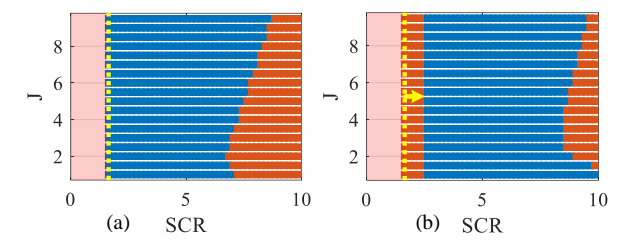


Fig. 4. *J* vs. SCR stability boundary curves for (a) VSG and (b) VSG+PLL. Blue and red dots indicate stable and unstable sampling points respectively.

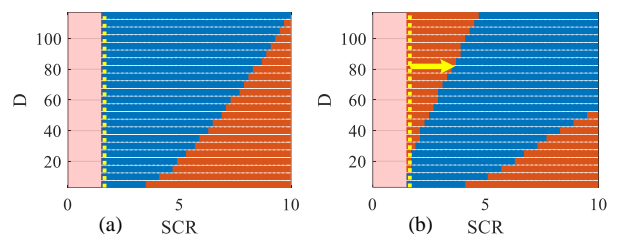


Fig. 5. \it{D} vs. SCR stability boundary curves for (a) VSG and (b) VSG+PLL.

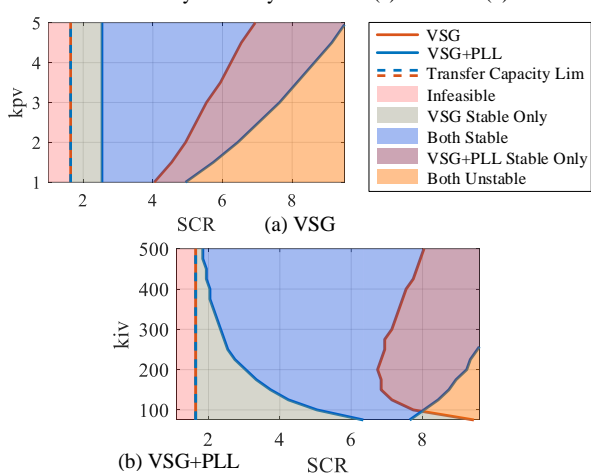


Fig. 6. Stability boundary curves of voltage controller parameters (k_{pv}, k_{iv}) .

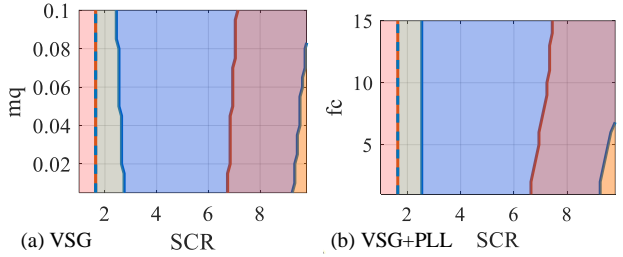


Fig. 7. Stability boundaries of Q-V droop (m_q , f_c).

deliver a specified amount of power and remains synchronized to the power system [15]. This arises from the fundamental principles of the two-machine system, which corresponds to the maximum grid impedance to transfer the set values of real and reactive power from one power source to the other for fixed voltage magnitudes.

Regions beyond that power transfer capability boundary are color-coded: the stable system is marked in blue; the unstable region is red. The *small-signal stability boundary line*, shown in Fig. 4, separates these stable and unstable areas. As expected, Fig. 4(a) shows VSG system stability worsens as SCR increases. The shape of the boundary line further suggests that the performance in strong grids can be improved by tuning the virtual inertia, especially since the curve does not vary monotonically i.e., the situation is the worst when *J* is around 2 pu. Fig. 4(b) shows that the red instability region of the VSG+PLL is shrunk, however, instability region also appears at low SCR, which introduces additional instability issue for weak grids with limited power transmission capacity.

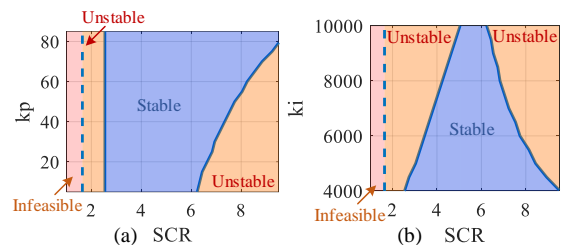


Fig. 8. (a) k_p or (b) k_i vs. SCR stability boundary curves for VSG+PLL.

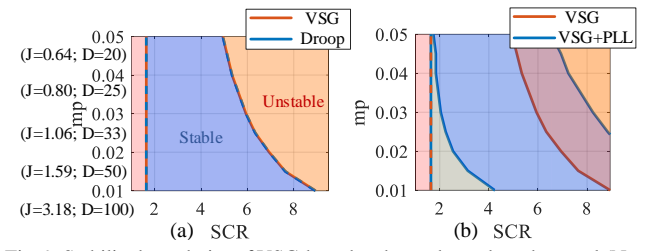


Fig. 9. Stability boundaries of VSG-based and P- ω droop-based control (Note that the cut-off frequency f_c is listed in Table I).

In other words, the well damped system improves the stability performance in strong grids, whereas it becomes unstable in weaker grids due to the structure of PLL.

Fig. 5 further examines the boundary variation of damping factor *D* that is directly related to the damping loop of VSG control. As seen in Fig. 5(a), the stability of typical VSG system worsens as *D* decreases [5], reflected in the expanding red region. Consequently, a higher value of *D* is required as the grid becomes stronger. Fig. 5(b) features a similar yet improved trend, where the VSG+PLL performs well even at very high grid strengths (e.g., SCR in the range of 8-10) if *D* is larger than 60. It is worth noting that increasing *D* has a dual effect, it improves performance in strong grids but negatively affects the stability in weaker grids, which reveals a trade-off between these competing factors. Moreover, for VSG+PLL, tuning *J* is effective for strong grids only, while *D* benefits both weak and strong grids.

C. Sensitivity analysis: voltage controller and Q-V droop

The integration of the PLL only modifies the damping loop; the voltage and *Q-V* droop controllers remain the same control structure. The stability characteristics of these controller parameters are presented in Fig. 6 and 7. In the subsequent stability boundary plots, the boundary lines of the two models are merged together for simplicity. As the different stability performance, there are five different regions illustrated: the infeasible region limited by power transfer capability, the stable region for VSG only, the stable region for both models, the stable region for VSG+PLL only, and the unstable region for both models. This region identification also helps to form a strategy for enhancing stability via switching between the two damping methods.

Fig. 6(a) shows that increasing k_{pv} from 1 to 5 expands the VSG stability range (red solid line) from 4 to 6.9 SCR, and using PLL (blue solid line) extends that range from 5 to 9.5 SCR. The VSG+PLL boundaries reaffirm the drawback of PLL – loss of stability in weaker grids – while noting that variations in k_{pv} have less impact on this region. The combined region plot further indicates that for SCR values above 4, the PLL damping method offers better performance, while in weaker grids, the typical VSG is the preferred choice.

In Fig. 6(b), the VSG system exhibits the worst stability when k_{iv} is adjusted to 200, and the system tends to be unstable at SCR=6.7. The k_{iv} plays an important role in VSG+PLL system; the higher its value, the better the stability, e.g., if it is

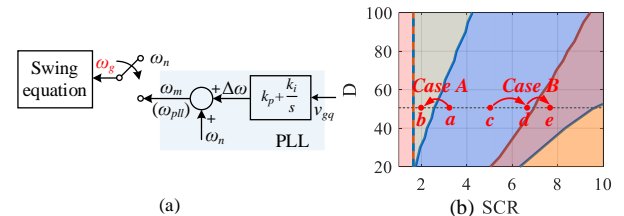


Fig. 10. Case studies overview: (a) subsystem of ω_g ; (b) Operating Points.

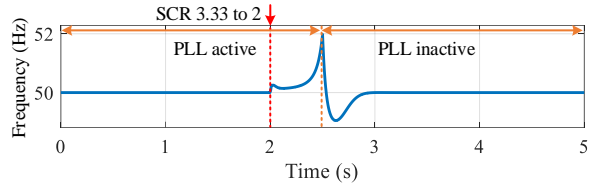


Fig. 11. Simulation of VSG+PLL system as SCR is reduced at 2 s and PLL damping loop is deactivated at $2.5\ s.$

increased to 500, the system is stable at most grid strengths. It also warns that the use of PLL damping loop is not always a good choice for strong grids.

Fig. 7 considers the parameters in Q-V droop control and reveals that increasing the m_q and f_c within a reasonable range enhances stability for both damping systems. Again, it shows that the VSG+PLL is vulnerable to weak grids (although it can be slightly improved by adjusting m_q); whereas it performs well in stiff grids, as shown in Fig. 7, where the red regions are significantly reduced to the yellow ones.

D. Sensitivity analysis: k_p and k_i of PLL

In order to explore the effect of PLL on the VSG+PLL variant, sensitivity analyses of the controller gains are shown in Fig. 8. When k_p increases, the stable region in strong grids is extended from SCR 6.2 to 10, while the system unstable behavior in weak grids is less affected. Fig. 8(b) shows that an increase in k_i reduces the feasible SCR stability range, similar to the eigenvalue trajectory sensitivities analyzed in [9]; for example, if $k_i = 10000$, the range is minimized to (5, 6.2).

E. Comparision with droop-based control

The aforementioned equivalence between VSG and frequency droop-based control follows from the swing equation, with assumptions of a constant grid frequency and active power set-points [10]. Fig. 9 shows the resulting curves obtained by varying P- ω droop coefficient m_p and setting the values of J and D as defined in equation (5): the boundary curves for both controllers perfectly match. In Fig. 9(a), it is clear that GFM exhibits better performance in weak grids. The shape of boundary lines first implies that a higher m_p can efficiently improve GFM stability, which agrees with observations in [3]; it also verifies the equivalence of the two GFM controls. The boundary deviations in Fig. 9(b) reveal again the effect of introducing the PLL.

IV. TIME-DOMAIN RESULTS

In accordance with the stability boundaries mentioned above, two case studies are simulated in time domain in this section. The system is similar to the previous analyzed model, only the damping loop is modified to use a switching component to deactivate (using the nominal frequency ω_n) or activate PLL. Fig. 10(a) shows the subsystem used to derive ω_g , as referenced in Fig. 2(a). The stability of the system under different grid strengths is tested. Fig. 10(b) shows two case studies, A and B, in which one transition is from operating point a to b, and the other from c to e. The system was simulated in MATLAB/Simulink with parameters as outlined in Table I.

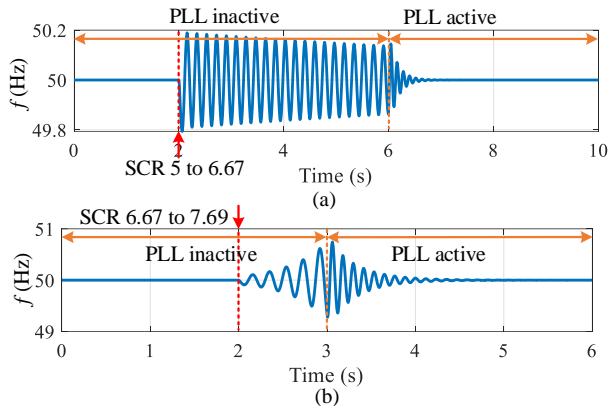


Fig. 12. Simulation of typical VSG system as SCR and damping loop change.

A. Case studies in weaker grid

The weaker grid case (*Case A*) in Fig. 10(b) is investigated first for the simple case where the typical VSG always shows stable operation, but VSG+PLL introduces instability issues. In this case, the VSG system with activated PLL damping starts to operate and the SCR suddenly drops from 3.33 to 2 at t=2s, thus crossing the boundary point 2.53 mentioned in Section III. The time-domain simulation results in Fig. 11 show that the system frequency loses stability and rises to 52 Hz in only 0.5s. After t=2.5 s, the PLL unit is deactivated, and the frequency re-stabilizes at 50 Hz. The time-domain results are consistent with theoretical analysis, which proves that the PLL employed in the damping unit of VSG has a negative impact on the stability of weaker grids.

B. Case studies in stronger grid

Fig. 10(b) illustrates the stronger grid test cases, moving first from point c to d as the SCR rises from 5 to 6.67, though it remains below the boundary point of 6.93 noted earlier. The system is initially operated with ω_n , then applies the SCR change at t=2s and activates the PLL at 6s. The results in Fig. 12(a) demonstrate that the typical VSG system can remain stable after the grid impedance change but is poorly damped, while activating the PLL loop results in faster reduction of frequency oscillations. Fig. 10(b) reconfirms this, i.e., both operating points are located in the "Both Stable" region, and thus both systems are stable; it further emphasizes the PLL's role in aiding damping.

Fig. 12(b) shows that the typical VSG system tends to be unstable when SCR is further increased to 7.69. At 3 s, the PLL damping loop is activated, which re-stabilizes the frequency. This suggests that properly enabling or disabling of the PLL in damping loop can prevent system from instability (as seen in Fig. 11 and 12), leading to the interesting concept of adaptively switching the PLL. The boundary lines and mapped regions thus play a vital role in helping to form the damping loop tuning strategies that allow the inverter to perform optimally under different grid strengths.

V. CONCLUSION

In this paper, the stability of VSG with different damping methods is investigated. The stability boundary serves as a visual tool for defining the basic criteria for parameter adjustments, which maps the boundaries using a 'grid-search' manner. By combining sensitivity analysis of controller parameters and grid impedance, the results identify the power transfer capability and small-signal stability boundaries, highlighting the system's physical limitations and stability margins, respectively. The suggested feasible regions show that the introducing PLL in the damping loop has a dual effect

on stability, i.e., it enhances the VSG damping behavior in the stiff grids, but also leads to instability in weak grids. It also validates the feasibility of applying a damping-switching method through PLL activation/ deactivation in time domain simulation. Further work will apply this analysis to develop an online damping tuning method based on real-time grid impedance estimation and validate it in hardware experiments. Furthermore, the detailed multi-level inverter systems and advanced grid strength metrics can substitute single-bus and traditional SCR metrics to improve root cause identification and system behavior evaluation.

ACKNOWLEDGMENT

This work has been conducted within UNIFORM project and supported by UKRI under Grant agreement EP/Y001575/1. It was also financially supported by ROSES project under Grant Agreement EP/T021713/1.

REFERENCES

- [1] X. Gao, D. Zhou, A. Anvari-Moghaddam and F. Blaabjerg, "Stability Analysis of Grid-Following and Grid-Forming Converters Based on State-Space Modelling," *IEEE Trans. Ind. Appl.*, vol. 60, no. 3, pp. 4910-4920, May-June 2024.
- [2] X. Luo, A. G. Paspatis, A. K. Singh, N. Hatziargyriou and E. I. Batzelis, "Modeling of DC-Side Dynamics in PV/Battery Grid-forming Inverter Systems," in 2023 IEEE Power & Energy Society General Meeting (PESGM), Orlando, FL, USA, 2023.
- [3] N. Pogaku, M. Prodanovic and T. C. Green, "Modeling, Analysis and Testing of Autonomous Operation of an Inverter-Based Microgrid," *IEEE Trans. Power Electron.*, vol. 22, no. 2, pp. 613-625, March 2007.
- [4] M. Ebrahimi, S. A. Khajehoddin and M. Karimi-Ghartemani, "An Improved Damping Method for Virtual Synchronous Machines," *IEEE Trans. Sustain. Energy*, vol. 10, no. 3, pp. 1491-1500, July 2019.
- [5] J. Liu, Y. Miura, and T. Ise, "Comparison of dynamic characteristics between virtual synchronous generator and droop control in inverterbased distributed generators," *IEEE Trans. Power Electron.*, vol. 31, no. 5, pp. 3600-3611, May 2016.
- [6] C. Li, Y. Yang, Y. Cao, A. Aleshina, J. Xu, and F. Blaabjerg, "Grid inertia and damping support enabled by proposed virtual inductance control for grid-forming virtual synchronous generator," *IEEE Trans. Power Electron.*, vol. 38, no. 1, pp. 294-303, Jan. 2023.
- [7] S. Jiang and G. Konstantinou, "Dual Influence of Power-Synchronization Loop on the Stability of Virtual Synchronous Generators," in 2023 IEEE Int. Future Energy Electron. Conf. (IFEEC), Sydney, Australia, 2023, pp. 6-11.
- [8] Y. Zhang, Q. Sun, J. Zhou, L. Li, P. Wang, and J. M. Guerrero, "Coordinated control of networked AC/DC microgrids with adaptive virtual inertia and governor-gain for stability enhancement," *IEEE Trans. Energy Convers.*, vol. 36, no. 1, pp. 95–110, Mar. 2020.
- [9] Y. Zhou, X. Xiong, X. Li, and P. Cheng, "Effects of PLL in the damping unit of a gird-connected VSG," in 2022 IEEE Int. Power Electron. Appl. Conf. Expo. (PEAC), 2022, pp. 589–593.
- [10] S. D'Arco and J. A. Suul, "Equivalence of virtual synchronous machines and frequency-droops for converter-based microgrids," *IEEE Trans. Smart Grid*, vol. 5, no. 1, pp. 394-395, Jan. 2014.
- [11] Y. Li, Y. Gu, and T. C. Green, "Revisiting grid-forming and grid-following inverters: A duality theory," *IEEE Trans. Power Syst.*, vol. 37, no. 6, pp. 4541-4554, Nov. 2022.
- [12] W. Du, et al., "Virtual Synchronous Machine Grid-Forming Inverter Model Specification (REGFM B1)," 2024.
- [13] F. Gao and M. R. Iravani, "A control strategy for a distributed generation unit in grid-connected and autonomous modes of operation," *IEEE Trans. Power Delivery*, vol. 23, no. 2, pp. 850-859, Apr. 2008.
- [14] X. Luo, G. Saridaki, A. K. Singh, P. Kotsampopoulos and E. I. Batzelis, "Stability boundary analysis of grid-forming and grid-following inverters," in 14th Mediterranean Conf. Power Gener., Transmiss., Distrib. Energy Convers. (MEDPOWER'24), Athens, Greece, 2024.
- [15] L. Huang, C. Wu, D. Zhou, and F. Blaabjerg, "A double-PLLs-based impedance reshaping method for extending stability range of gridfollowing inverter under weak grid," *IEEE Trans. Power Electron.*, vol. 37, no. 4, pp. 4091-4104, Apr. 2022.